POSITIVE CONSTRAINED ITERATIVE DECONVOLUTION ALGORITHM APPLIED TO THREE-DIMENSIONAL IMAGES OF FLUORESCENCE MICROSCOPY

J. E. Diaz-Zamboni, E.V. Paravani; N. B. Vicente, J. F. Adur; V. H. Casco*
Laboratorio de Microscopia, Facultad de Ingeniería, Universidad Nacional de Entre Ríos
Ruta 11, Km 10½ CC 47. Suc. 3 (3100) Paraná, Entre Ríos. Argentina.
Fax: (54 – 343) 4975100/101.
*** Correspondence author: VHC** vcasco@bioingeneria.edu.ar

Summary

Cellular and molecular biology seek to understand complex cellular functions and cell interaction with the environment. To achieve this, different real-time and in situ processes must be described. Digital deconvolution microscopy is one of the most powerful tools used previous to the analyses and quantification of cell molecules. It uses the microscopy system's optical transfer function to quantify the image degradation produced by lens aberrations. The deconvolution process allows the reconstruction of three-dimensional images that can be then visualized and quantified. The quality of three-dimensional reconstruction depends on the type of deconvolution algorithm used. Linear deconvolution algorithms have shown to be useful when high processing speed is necessary. However, the inversion process involved produces noise amplification. On the other hand, iterative algorithms are more realistic since they work on an estimator that permits the quantification of the level of restoration achieved in every cycle. In this paper we show the results of an evaluation of a particular implementation of an iterative algorithm based on the Van Cittert update scheme. The algorithm was tested on images of biological specimens. Results obtained show that the algorithm conserves intensities, decreases low frequency information and does not amplify high frequencies.

Key words: Deconvolution, transfer function, iterative algorithm, three-dimensional reconstruction.

Introduction

Three-dimensional (3-D) images formed by fluorescence wide-field microscopy are characterized for containing mainly light from the whole volume (information in focus and out of focus), in addition to acquisition system noise and auto-fluorescence (Wallace, 2001). This makes it difficult to distinguish true fluorescent signals and the right focal plane to which they belong. An important practical rule to obtain good 3-D microscopy images is to reduce optical aberrations. Techniques such as Confocal Laser Scanning Microscopy (CLSM), reduce out of focus fluorescence physically by using a pinhole of between 0.1 and 0.7 mm of diameter. In this setup, only fluorescence coming from confocal planes is detected (Shotton, 1993).

Digital Deconvolution Microscopy (DDM) is a computational technique used to improve the contrast and resolution of digital images. It includes a suite of methods that seek to remove blur –eliminating intensities– or restore the out of focus contributions –reassigning intensities– present in microscopy images caused by the limited numerical aperture of the objective lens (Wallace, 2001).

In order to ensure the best performance of the mentioned methods, it is important to have a good characterization of the out of focus fluorescence. This is achieved by obtaining the Point Spread Function (PSF) of the system, that is to say its transfer function, which contains the information of the distortion of an infinitesimal point source of light. Therefore, specimens can be deconvolved using this information since they can be considered as an infinite set of points. The PSF can be obtained by three different techniques: experimental, analytical and computational. In the former, images of one or more point-like objects are collected and used to obtain the PSF. In the case of analytical methods, the PSF is calculated using a classical diffraction based model. In the latter, computational algorithms, such as blind deconvolution, are used to estimate the PSF (P. Sarder, 2006).

The experimental PSF's conditions must match closely the setup used to obtain the specimen's 3-D image, which is an optimum condition for deconvolution (Wallace, 2001). It is determined using the image of a point source of light which consists of fluorescent latex micro-spheres of known diameter which are smaller than the first dark ring of the diffraction pattern. In 3-D space, this phenomenon is observed as a solid of revolution with bi-conical shape, which has a vortex in the centre.

Deconvolution algorithms used by DDM derive from the mathematical analysis which describes the microscope's image-formation process. This process is the convolution of two variables: the known 3-D PSF $s(x,y,z)$ and a unknown variable which is the original spatial distribution of light in the 3-D specimen $o(x,y,z)$ (Castleman, 1996; Jansson, 1997; McNally, 1997; Sibarita, 2005). This optical phenomenon can be mathematically described as follows:

$$i(x,y,z) = s(x,y,z) \otimes o(x,y,z) \tag{1}$$

where $i(x,y,z)$ is the 3-D image captured by optical sectioning and $\otimes$ is the 3-D convolution operator.

The general philosophy of iterative algorithms is to estimate a solution $\hat{o}(x,y,z)$ which produces the 3-D image $i(x,y,z)$ when convolved with $s(x,y,z)$ (Sibarita, 2005). That is to say:

$$i(x,y,z) = s(x,y,z) \otimes \hat{o}(x,y,z) \tag{2}$$

However, in practice, additive noise reduces the equality of Equation (2) to the best approximation.

In the implementation of the present algorithm $\hat{o}(x,y\ z)$ was searched via an algebraic update method (Jansson, 1997). The positivity constraint was selected as restriction criteria for the update process in each cycle since the estimator can not have negative values. This is due to the fact that images containing fluorescence signals are always non-negative (Jansson, 1997; Agard, 1984).

The convergence of the method is achieved by calculating the estimation error $R^{(k)}$ in each k cycle.

$$R^{(k)} = \frac{\sum_{x,y,z} \left| i(x,y,z) - \hat{i}^{k}(x,y,z) \right|}{\sum_{x,y,z} i(x,y,z)} \tag{3}$$

where :

$$\hat{i}^{(k)} = s(x,y,z) \otimes \hat{o}^{(k)}(x,y,z)$$

$R^{(k)}$ provides only a method for convergence. Other parameters such as image contrast and frequency content must be used to evaluate the quality of restoration (Jansson, 1997). The algebraic-update method is based on the Van Cittert update scheme. The physical positivity restriction is also added to this scheme.

$$\begin{aligned} \hat{i}^{(k)} &= s(x,y,z) \otimes \hat{o}^{(k)}(x,y,z) \\ \hat{o}^{(k+1)} &= \hat{o}^{(k)}(x,y,z) + \left[i(x,y,z) - \hat{i}^{(k)}(x,y,z) \right] \\ &\text{if } \hat{o}^{(k+1)} < 0, \text{ then } \hat{o}^{(k+1)} = 0 \\ k &= k+1. \end{aligned} \tag{4}$$

Equation (4) shows the algorithm's step by step sequence. The starting point is $k = 0$, where $\hat{o}^{(0)}(x,y,z) = i(x,y,z)$, since $i(x,y,z)$ is a good first approach to the specimen. In the first step, $i^{(k)}(x,y,z)$ is determined by the convolution of the estimated object with the PSF. This process results in the blurring of $i^{(k)}(x,y,z)$. Then, the following step is to estimate $\hat{o}^{(k+1)}(x,y,z)$, which is obtained by summing the difference between the 3-D image captured, $i(x,y,z)$, and $i^{(k)}(x,y,z)$ to $\hat{o}^{(k)}(x,y,z)$. $\hat{o}^{(k+1)}(x,y,z)$ is a version of $\hat{o}^{(k)}(x,y,z)$ corrected by the mentioned term; in defocused zones, $\hat{o}^{(k+1)}(x,y,z)$ tends to be negative since $i^{(k)}(x,y,z)$ is generally greater than $i(x,y,z)$ making the term between brackets negative. On the other hand, small differences in the mentioned term are present only in zones where the 3-D image is highly contrasted, that is to say, focused zones. Ideally, the term between brackets is modulated by a relaxation function which weights it voxel-wise, preventing abrupt changes. Additionally, the positivity constraint ensures there are no negative values in the estimator by assigning them a value of zero in each new cycle. This mode of imposing limits is a very robust approach, even in the presence of noise (Jansson, 1997).

In this paper, we show the performance evaluation of an implementation of the algorithm (Diaz-Zamboni, 2004). Speed of execution is tested using different biological specimens. Convergence error is analyzed considering different number of iterations. Spatial frequency components of deconvolved images are analyzed qualitatively in order to obtain a measure of the restoration quality.

Materials and Methods

Microscopy System

The system used was developed in our laboratory. It is based on an Olympus BX50 upright microscope equipped with both an UV lamp for epi-fluorescence and a halogen lamp for transmitted light. The recording system consists of an Apogee CCD camera model AM4, attached to the microscope using a 0.5x mount-C lens, sensor of 768x512 pixel^2, square pixels with sides 9 micrometers long, 14 bits of resolution and cooling system. In addition, a stepping motor RS 440-436 was connected to the micrometric screw of the microscope via a 100:1 reducing box (Adur and Schlegel, 1997).

Software

We developed a software called SUMDD (from the Spanish: *Software para Usuarios de Microscopía de Desconvolución Digital*) (Diaz-Zamboni, 2004), which controls both the camera via an ISA card and the stepping motor via parallel port, allowing image capture, focusing by keyboard, optical sectioning, 3D deconvolution and visualization.

SUMDD was implemented in Object Pascal language, and it has various modules to do the mentioned tasks. For the present work, the deconvolution module was modified to count and measure the duration of the iterations of the algorithm under study. These consisted on adding a routine that logs the time at the beginning and at the end of the algorithm execution and a counter that stops the algorithm after a determined amount of iterations.

Maximum intensity projection (MIP) was used to visualize 3-D information. SUMDD allows rendering raw and deconvolved 3-D images at the same time using MIP for comparison (Chen et al., 1995).

Calculation and Visualization Module

The module used to perform calculations is a personal computer INTEL Pentium IV, 640 MB RAM, video adapter nVIDIA TNT2 32 MB RAM, Windows NT4.0 operative system. SUMDD is also installed in this module. This computer allows to do deconvolution and the 3-D visualization of data.

PSF Determination

Fluorescent beads were optically sectioned in order to obtain the PSF. They were selected to be close to the resolution limit of the microscope. They were optically sectioned from bottom to top following modified Kozubek's protocols (Kozubek, 2001). Two PSFs were determined, one for 10x and one for 20x. Each image was an average of three captures, which were then background corrected. Images were finally stored in TIFF format in gray scale with 8 bits of resolution.

Specimens

Two different biologic models were used. These have been thoroughly studied, and today they are considered as important models by many researchers. Porcine hepatic spheroids (Fiorucci, 2003) in which the distribution pattern of apoptotic bodies has been analyzed

and quantified (Lavin, 1993), and embryos of *Bufo arenarum* in which the expression of cell adhesion molecules in the skin has been analysed (Izaguirre, 2000).
Porcine hepatic spheroids were selected from a set, fixed with 4 % formaldehyde in 0.1 M PBS pH 7.2 and stored at 4°C. They were washed with PBS 1X, permeated with Triton 0.1% X-100 and 0.1% Sodium Citrate for 25 minutes, then washed again twice with PBS 1X. TUNEL reactions were carried out according to the supplier's instructions (Boehringer Mannheim GmbH. In situ cell death detection fluorescein kit). Next, the spheroids were washed three more times with PBS 3X, so that possible aqueous remnants were eliminated. Finally, spheroids were mounted with Vectashield (Vector) and stored at 4°C.
For the localization of E-cadherin complete stage 19 embryos *Bufo arenarum* were used (Paddock, 1999). They were fixed in Carnoy, washed with PBS 1X at room temperature and treated with Triton X-100 (SIGMA) 0.1% PBS during 30 minutes at room temperature. Specimens were incubated with normal goat serum 1:20 during 35 minutes and anti-E-cadherin rat primary monoclonal antibody; (anti-E-cadherin Transduction Laboratories, Lexington, USA), used to identify the 120 KDa isoform of E-cadherin 1:50 to 37° C during 75 minutes. After the incubation, embryos were washed in PBS and incubated with the secondary antibody (rabbit IgG-FICT anti-rat, SIGMA) and mounted in anti-fading solution (Vectashield, Vector Laboratories). As negative control the primary antibody incubation was omitted.
Porcine hepatic spheroids and *Bufo arenarum* embryos were optically sectioned with a 10x and 20x objective lens, respectively, in both cases producing 128x128x16 stacks.

Algorithm Evaluation
In order to evaluate the algorithm's convergence, the deconvolution method was run for 10, 50 and 100 iterations by triplicate for each specimen. At the end of each process, the error of convergence was determined.
Changes in resolution were estimated using the Discrete Fourier Transform (DFT) of 3-D raw and deconvolved images, which was applied to raw and deconvolved stacks. Instead of an array of pixels the DFT is set of elements which represent an image as a sum of sine waves of different frequencies, amplitudes and directions. This is referred to as the frequency domain or Fourier representation where the *spectral information* is present. 3-D images (raw and deconvolved) were transformed with the Fast Fourier Transform (FFT) which is an algorithm to efficiently obtain the DFT (Castleman, 1996; Horgan et al., 2000). Lines were traced in each transformed 3-D image, corresponding spatially in both volumes –raw and deconvolved– and were represented in a bi-dimensional (2-D) graph. Low frequencies –which appear at the centre of the graph– and high frequencies –extending to both sides of the graph– were analyzed; these correspond to out of focus information and noise, respectively.

Results

In order to obtain a measure of the convergence evolution, $R^{(k)}$ was evaluated for three different number of iteration. Tables I and II, show these results for two specimens, E-cadherin in *Bufo arenarum* skin and apoptotic bodies in porcine hepatic spheroids, respectively. In both cases as the amount of convergence error decreases asymptotically. That is to say, values of convergence error reach an equilibrium that is imposed by the difference term in the second step of Equation (4).

Image intensity conservation can be distinguished comparing deconvolved and raw 3-D images in gallery views. Figures 1 and 2 show these results, the upper rows show raw stacks while lower rows contain deconvolved stacks. Highly contrasted zones have the same intensity level in both series views while on the other hand, zones where defocused information is present there is less intensity in the deconvolved stack.
Figures 3 and 4 show spatial frequency profiles that were obtained transforming the 3-D images to Fourier domain, then tracing a line in the resultant transformed volumes (raw and deconvolved) and representing them in a 2-D graph. Raw data is shown with a continuous line and deconvolved data with a dotted one. In these profiles it is evident that out of focus information (corresponding to low frequencies, in the central zone of the graphs) have decreased and high frequencies (at both sides of the figures) are conserved.
Figures 5 and 6 show maximum intensity projections of raw and deconvolved stacks, which is one of the most used visualization schemes for 3-D reconstruction of biological specimens that has been labelled by immuno-fluorescence reactions. Comparing the raw and deconvolved data projections (left and right, respectively) it is clear that out of focus information has been reduced in deconvolved stacks; out of focus information interferes with the correct visualization of structures behind it.

Conclusions

Optical sections analyses and profiles of magnitude spectrum of the 3-D images showed that the algorithm does not amplify noise and it preserves high frequency information, which implies that the limit of optical resolution of the system (Jansson, 1997) is conserved. This takes even more relevance since the present paper showed similar numerical results, independently of the experimental model used. Consequently, the strength and stability of the developed algorithm are corroborated.
Results also show that a method may be created to ameliorate the implementation of the algorithm. This method should control improvements in the frequency domain, that is to say, low frequency depletion and high frequency conservation.
The iterative method presented is reasonably fast and is robust stability-wise. The availability of powerful personal computers allows to process large amounts of data and to obtain 3-D images with high resolution, comparable with those obtained with CLSM. This method is readily applied to images with different wavelengths, as long as the corresponding PSF for the new wavelength is calculated.
From the results we can infer that the iterative deconvolution algorithm with positive restriction maintains the intensity of pixels that are effectively in focus (highly contrasted zones). It is highly recommended that any 3-D quantification tool is applied to restored stacks, since stacks deconvolved with restoration algorithms preserve intensities as opposed to deblurred ones.
The technological improvements developed in 3-D microscopy made by our group require the continuous evolution of the software for 3-D image analyses and processing. With the implementation of this algorithm for 3-D fluorescence microscopy images, we can offer another important tool to perform cell and molecular biology studies.
Since that approach was used in two different biological models, and in both cases the algorithm behaviour was similarly robust, it can be a cheaper choice for microscopy laboratories.

References

[1] Wallace W., Schaefer L. H., Swedlow J.R. (2001). "A workingperson's guide to deconvolution in light microscopy". *Biotechniques*. 31(5) : 076–1097.
[2] Shotton D., (1993). "Electronic light microscopy. Techniques in Modern Biomedical Microscopy" 1st ed. 605 Third Avenue, New York, USA. Wiley-Liss.
[3] Sarder P., Nehorai A. (2006). "Deconvolution Methods for 3-D Fluorescence Microscopy Images". *IEEE Signal Processing Magazine*. 23(3) : 32-44.
[4] Castleman K. R., (1996). "Digital image processing" 1ra ed. New Jersey. Prentice Hall.
[5] Jansson P., (1997). "Deconvolution of images and spectra" 2nd ed. 1300 Boylston Street, Chestnut Hill, MA 02167, USA. Academic Press.
[6] Mcnally J.G., Karpova T., Cooper J., Conchello J.A. (1999). "Three-dimensional imaging by deconvolution microscopy". *Methods*. 19 : 373–385.
[7] Sibarita J.B. (2005). "Deconvolution Microscopy". *Adv Biochem Eng Biotechnol*. 95 : 201-243.
[8] Agard D.A. (1984). "Optical sectioning microscopy: Cellular architecture in three dimensions". *Annu Rev Biophys Bioeng.* 13 : 191–219.
[9] Diaz-Zamboni J.E. (2004). "Software para usuarios de microscopios de desconvolución digital". Thesis Degree. Facultad de Bioingeniería, Universidad Nacional de Entre Ríos.
[10] Adur J.F., Schlegel J.O. (1997). "Diseño, desarrollo y construcción de un sistema de avance micrométrico para microscopios fotónicos". Thesis Degree. Facultad de Bioingeniería, Universidad Nacional de Entre Ríos.
[11] Kozubek M. (2001). "Theoretical versus experimental resolution in optical microscopy". *Microsc Res Tech*. 53: 157-166.
[12] Fiorucci M.P., Izaguirre M.F., Lorenti A., Hidalgo A., Ielpi M., Argibay P., Casco V.H. (2003). "Expresión de moléculas de adhesión celular en organoides hepáticos desarrollados para funcionar en un hígado bioartificial". In: *XIV Congreso Argentino de Bioningeniería. III Jornadas de Ingeniería Clínica. Sociedad Argentina de Bioingeniería*. pp. 29.
[13] Lavin M., Watters D., Eds (1993). "Programmed cell death: The cellular and molecular biology of apoptosis" 1st ed. Emmaplein 5, 1075 AW Amsterdam, The Netherlands. Hardwood Academic Publishers.
[14] Izaguirre M.F., Peralta-Soler A, Casco V.H. (2000). "Induction of morphological alterations mediated by e-cadherin and α-catenin antibodies in Bufo arenarum (anura - bufonidae)". *Histol Histopathol*. 4(16): 1097–1106.
[15] Horgan G.W., Reid C.A., Glasbey C.A. (2000). "Biological image processing and enhancement". In: Image processing approach. Eds., R. Baldock and J. Graham. In: The practical approach series. Series Ed., B.D. Hames. 219: 37-66.
[16] Walker J.M., (1999). "Confocal microscopy. Methods and protocols. In: Methods in molecular biology" 1st ed. 999 Riverview Dirive, Suite 208 Totowa, New Jersey 075512, USA. Humana Press.
[17] Chen H., Swedlow J.R., Grote M., Sedat J.W., Agard D.A., (1995). "The collection, processing and display of digital three dimensional images of biological specimens. In: Handbook of biological confocal microscopy" 2nd ed. J. B, Pawley Ed. Plenum Pres, New York. 197-210.

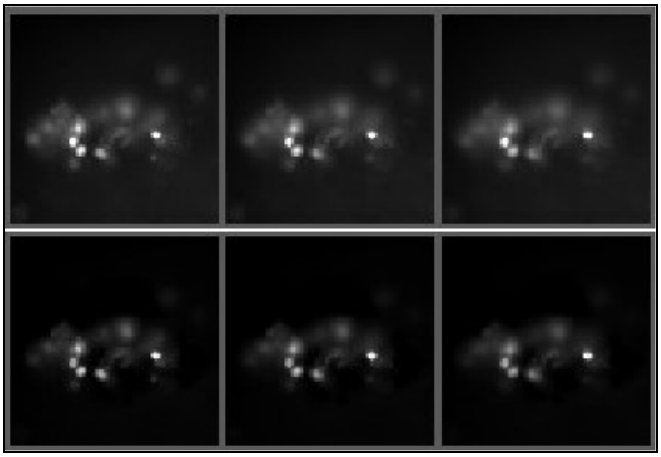

Figure 1. Optical sections of apoptotic bodies in porcine hepatic spheroids. Signal obtained by TUNEL.

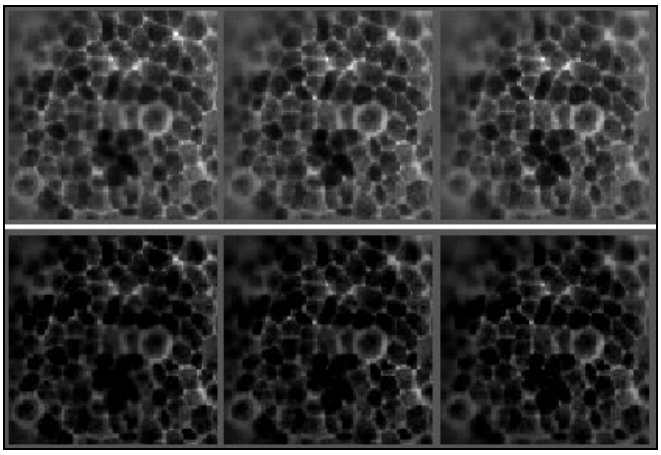

Figure 2. Optical sections of *Bufo arenarum* skin, where E-cadherin expression was obtained with immuno-fluorescence techniques.

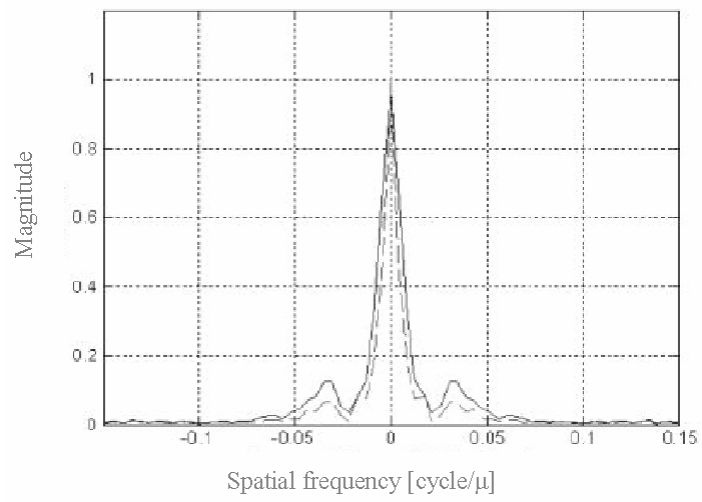

Figure 3. Spatial frequency profiles of apoptotic bodies in porcine hepatic spheroids, where apoptotic bodies were detected (raw and deconvolved images in continuous and dotted lines, respectively).

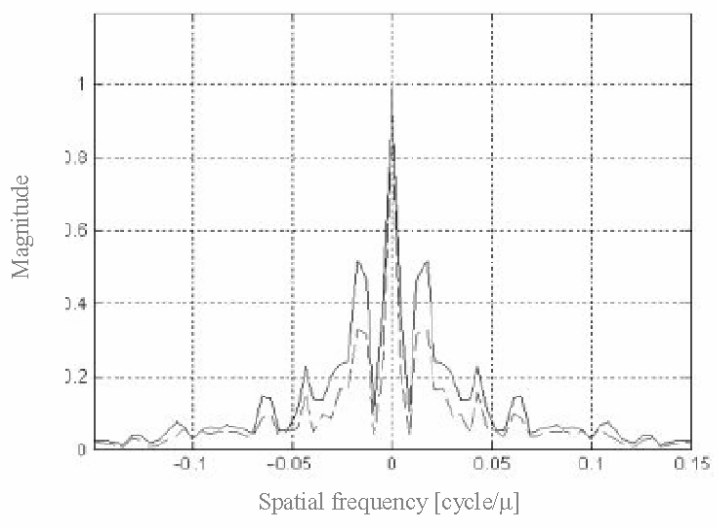

Figure 4. Spatial frequency profiles of E-cadherin expression in *Bufo arenarum* skin (raw and deconvolved images in continuous and dotted lines, respectively).

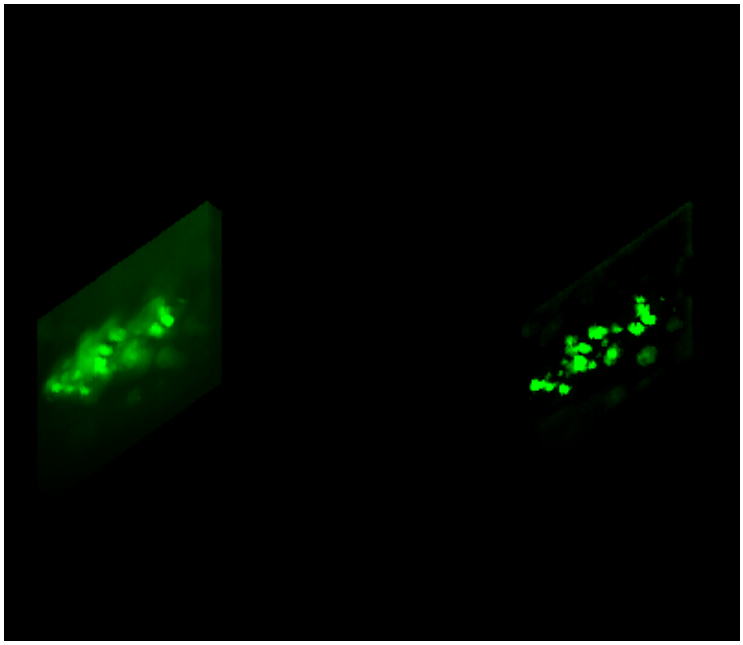

Figure 5. Maximum intensity projection of apoptotic bodies in porcine hepatic spheroids.

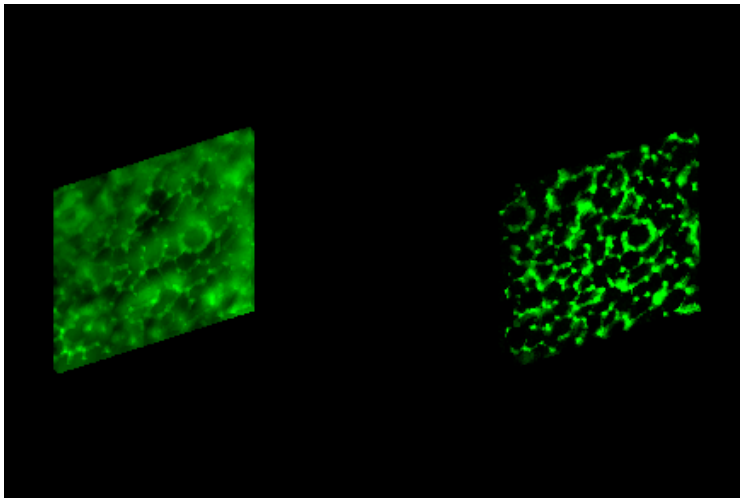

Figure 6. Maximum intensity projection of E-cadherin expression in *Bufo arenarum* skin.

Table I

Iteration number	Time [min] mean± SD	Error [%]
10	0.4222±0.22	0.700
50	3.10±0.01	0.081
100	6.09±0.04	0.080

Table I. Execution time and convergence error of the algorithm for different number of iterations. Test on porcine hepatic spheroids where apoptotic bodies were identified with the TUNEL technique.

Table II

Iteration number	Time [min] mean ± SD	Error [%]
10	0.4192±0.25	0.720
50	3.05±0.05	0.085
100	6.09±0.02	0.081

Table II. Execution time and convergence error of the algorithm for different number of iterations. Test on skin cells of *Bufo arenarum* where E-cadherin was identified.